Inorganic Chemistry

Article

pubs.acs.org/IC

Axial Thiophenolate Coordination on Diiron(III)bisporphyrin: Influence of Heme−Heme Interactions on Structure, Function and Electrochemical Properties of the Individual Heme Center

Debangsu Sil, Firoz Shah Tuglak Khan, and Sankar Prasad Rath*

Department of Chemistry, Indian Institute of Technology Kanpur, Kanpur-208016, India

Supporting Information

ABSTRACT: The binding of a series of substituted thiophenols as axial ligands on a highly flexible ethane-bridged diiron(III)bisporphyrin framework has been investigated as a model of diheme proteins. Spectroscopic characterization reveals a high-spin (S = 5/2) state of iron for all of the pentacoordinate thiophenolato complexes. In the UV−visible spectra of the complexes, the positions of the Soret and band I have been found to be dependent on the pK_a of thiophenols. The alternating shift pattern, which has opposite sign of the chemical shifts for meta- vs. ortho- and para- protons in the ^{1}H NMR spectra, is attributed to negative and positive spin densities, respectively, on thiophenolate carbon atoms and is indicative of π-spin delocalization to the bound thiophenolate ligand. The Fe(III)/Fe(II) redox couple of the complexes bears a linear relationship with the pK_a of thiophenol and is found to be positively shifted with decreasing pK_a. The effect of the electronic nature of the substituent on the thiophenolate ring has also been demonstrated in which a large potential range of 540 mV was observed (in contrast to the value of only 270 mV in case of monoheme analogues) for the Fe(III)/Fe(II) redox couple on going from monoheme to diheme and is attributed to the interheme interaction. Also, the Fe(III)/Fe(II) redox potential of the thiophenolato complexes has been found to be more positively shifted compared to their phenolato analogues, which was further supported by DFT calculation. The addition of another thiophenol at the sixth axial position of the five-coordinate thiophenolato complex causes a change in iron spin from high (S = 5/2) to low (S = 1/2) along with a large positive shift of 490 mV for the Fe(III)/Fe(II) redox couple.

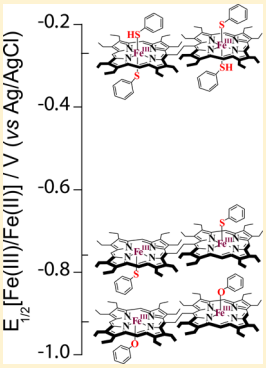

INTRODUCTION

Multiheme cytochrome *c* represents an extensive class of hemoproteins with a consequential role in electron transfer and enzymatic catalysis.[1] Understanding the importance of these motifs is critical for clarification of the highly optimized properties of multiheme cytochromes *c*; however, their spectroscopic investigation is often complicated by the presence of large numbers and efficient coupling of the individual heme centers.[1,2] The simplest member of such a family is the diheme cytochrome *c* (DHC2) from *G. sulfurreducens*, which has two different heme groups connected via a single polypeptide chain.[2] The observed differences in the porphyrin ring deformations between two heme centers and the axial ligand orientations in DHC2 have been proposed to be due to the heme−heme interactions, although the functional significance of these heme structural arrangements is yet to be understood. These attractive features have encouraged us to focus our investigation on the relationship between such interactions and the properties of the metal center as a part of our ongoing research.[3]

Sulfur coordination to heme-iron of multiheme is known to be an integral part of several biological proteins/enzymes.[4−7] For example, the photosynthetic reaction center (RC) from *Rhodpseudomonas viridis*;[4a] the triheme cytochrome c, DsrJ, from the purple sulfur bacterium *Allochromatium vinosum*;[4a] cytochrome c quinol dehydrogenase, NrfH, from the sulfate-reducing δ-proteobacterium *Desulfovibrio vulgaris*;[5] the diheme Cytochrome rC_{557} from *Escherichia coli*;[6a] bacterial diheme cytochrome *c* peroxidase;[6b] C_7-type three heme cytochrome (PpcA) from *G. sulfurreducens*;[6c] etc. are all multiheme cytochromes in which a sulfur atom coordinates to at least one heme center. The iron center of cytochrome P-450s (P-450) is also known to have a thiolate coordination.[7,8] Substrate binding at the active site of the P-450$_{cam}$ shifts the Fe(III)/Fe(II) redox potential to the positive side to be readily reduced by a physiological reductant. This regulation of the Fe(III)/Fe(II) redox potential is very crucial for P-450 to function in innumerable biological redox processes. The thiolate ligation is, therefore, expected to significantly influence the property of the heme iron. Until now, all the thiolato Fe(III) porphyrins studied as models of cytochromes have been with monohemes. The effect of such coordination on the diheme/multiheme cytochromes remains unexplored.

A covalently linked porphyrin dimer can be a useful model of the diheme centers. A sensible choice of the spacer will dictate the spatial arrangement, thereby allowing precise control over the inter-ring interactions and possible electronic communications. In the present work, two octaethylporphyrin rings have been covalently connected via a highly flexible ethane linker

Received: May 19, 2014
Published: November 6, 2014

dx.doi.org/10.1021/ic5011677 | *Inorg. Chem.* 2014, 53, 11925−11936

that supplements both the horizontal and vertical flexibility of the bisporphyrin system. Recently, we have reported very different structures and properties of Fe(III) complexes while using bisporphyrin architecture as compared to the corresponding monoporphyrin.[3] The complete reversal of the ligand field strength of ClO_4^- and $CF_3SO_3^-$ in the magnetochemical series has been observed in a diiron(III)bisporphyrin framework.[3a] Investigation of a series of phenolato diiron(III)bisporphyrins revealed the stabilization of pure intermediate-spin ($S = 3/2$) of iron in the 2,4,6-trinitrophenolato complex, while its monoporphyrin analog was found to stabilize the high spin state ($S = 5/2$) only.[3b] Our group also has reported recently a family of μ-hydroxo diiron(III)bisporphyrin in which two different spin states of Fe(III) are stabilized in a single molecular framework, even though both the cores have exactly the same chemical entity.[3g−i] All of these observations are believed to be the consequences of inter-ring interaction in dihemes.

The present work investigates the binding of a series of substituted thiophenols as axial ligands on a diiron(III)-bisporphyrin framework and compares with the corresponding monoporphyrin and phenolato analogues. Focus will be on how the inter-ring interactions in a porphyrin dimer influence the structure, electronic, and redox properties of the individual heme centers in contrast to its monoheme counterpart. The change in redox properties of the heme centers on going from a pentacoordinate to hexacoordinate complex will also be investigated. Density functional theory (DFT) calculations have been employed to rationalize the experimental observations in the present study.

RESULTS AND DISCUSSIONS

μ-Oxo-syn-1,2-bis[5-(2,3,7,8,12,13,17,18-octaethylporphyrinato)iron(III)]ethane, **1**, was synthesized using a procedure reported earlier.[3c] UV−vis spectroscopic data of **1** show a Soret band at 399 nm and Q-band at 579 nm in dichloromethane which suggest the face-to-face orientation of the porphyrin macrocycles. Upon the addition of thiophenol into the dichloromethane solution of **1**, a large change in the UV−visible spectra has been observed which results in an intense blue-shifted Soret band at 391 nm along with a shoulder at 413 nm, and three Q-bands arise at 511, 541, and 633 nm due to the formation of five-coordinate[9] complex **2a**. Similar spectral changes have also been observed for other thiophenolato complexes **2b−2d** reported here, and Figure 1 compares the UV−visible spectra between **1** and **2d** in dichloromethane. Scheme 1 shows the synthetic outline and list of the thiophenolato Fe(III)bisporphyrins reported here along with their abbreviations used.

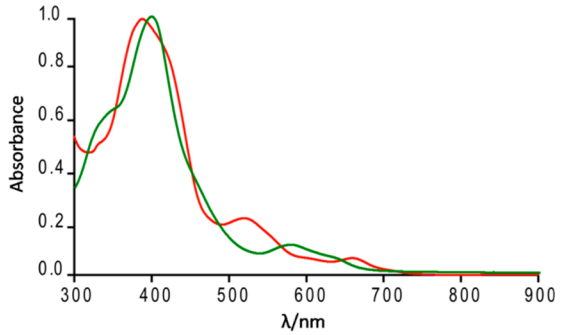

Figure 1. UV−vis spectra (at 298 K) of **1** (green line) and **2d** (red line) in dichloromethane.

UV−visible spectroscopy comes in handy, particularly in predicting the geometry of the thiophenolato complex in solution. Splitting of the Soret band is frequently discerned for the sundry porphyrin dimers and trimers in linear spatial orientations.[10] For example, splitting of the Soret band was obtained for the *anti* conformation of bis(zinc porphyrin) as a result of coordination of the axial ligands to the zinc ions.[10] Although the Soret band is not split into two distinct peaks in the present complexes, probably due to overlapping of $B_\perp$ and $B_\parallel$ transitions, a shoulder is seen to be accompanying the Soret band. The shoulder, although weak, indicates *anti* conformation in solution, which has been further confirmed by the single crystal X-ray structure (*vide infra*) in the solid. Dark purple crystalline solids of the molecules were deposited by slow diffusion of *n*-hexane into a benzene solution of the complexes in good yields and are structurally characterized. The solid state structures are also preserved in solution as reflected in the ^{1}H NMR spectra in $CDCl_3$ (*vide infra*). Detailed synthetic procedures of all the complexes along with their characterizations are given in the Experimental Section.

We also have synthesized a series of thiophenolato complexes of the mono-porphyrin analogues in order to compare with the related thiophenolato Fe(III)bisporphyrins reported here. Scheme 2 lists the thiophenolato Fe(III) porphyrin along with their abbreviations used in the present work. Although **4a** and **4b** were known previously, **4c** and **4d** are new. The difference in properties of the bisporphyrin complexes compared to the monoporphyrin counterpart would provide unequivocal evidence of the role played by inter-ring interactions in a porphyrin dimer.

The UV−vis spectral data for the Soret and Q-bands of the thiophenolato complexes **2a−2d** are summarized in Table 1. The wavelength maxima of the Soret and band I[8b] (~600−670 nm) for the complexes **2a−2d** have been plotted as a function of pK_a of thiophenols in Figure 2, which is found to be linearly correlated. Such linear correlation for the Soret band and band I have also been obtained for the thiophenolato complexes (**4a−4d**) of the monomeric counterpart. Band I has been assigned to porphyrin to iron, $a_{1u}(\pi)$ and $a_{2u}(\pi)$ to $e_g(d\pi)$, charge transfer transitions.[8b,c] With increasing electron donating ability of the ligand, the $d\pi$ orbitals of iron rise in energy and thereby shift the charge transfer transition to higher energy, i.e., shorter wavelength. A thiophenol with better electron donating ability, i.e., greater pK_a value, will increase the $d\pi$ energy level and, therefore, raise the charge transfer transition energy which eventually shift the absorbance to a shorter wavelength. A similar relationship was also observed earlier.[8b,12]

We also have plotted the wavelength maxima of the Soret and band I for the phenolato analog of the dihemes **5a−5e** (Chart 1) in Figure 2 as a function of pK_a of the substituted phenol. Although a similar trend to that described above has been obtained here also, a good fitting, however, was not obtained. It is interesting to note that a notably large deviation from linearity is observed in the case of **5d**, which is probably due to a change of iron spin state from a high (5/2) to intermediate spin (3/2) state.

Crystallographic Characterizations. Dark purple crystalline solids of the molecules were deposited by slow diffusion of *n*-hexane in a benzene solution of the complexes in the air at room temperature. Figures 3, 4, S2, and S3 demonstrate the X-

dx.doi.org/10.1021/ic5011677 | Inorg. Chem. 2014, 53, 11925−11936

Scheme 1

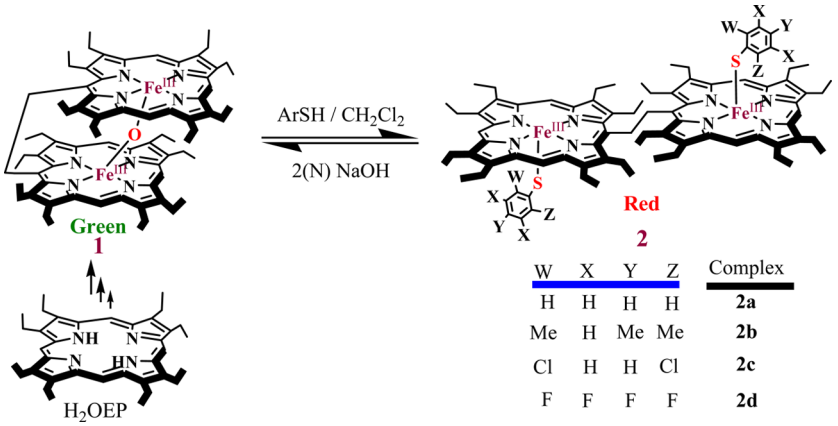

W	X	Y	Z	Complex
H	H	H	H	2a
Me	H	Me	Me	2b
Cl	H	H	Cl	2c
F	F	F	F	2d

Scheme 2

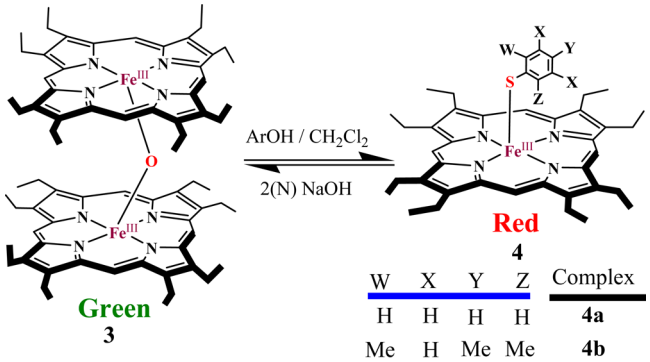

W	X	Y	Z	Complex
H	H	H	H	4a
Me	H	Me	Me	4b
Cl	H	H	Cl	4c
F	F	F	F	4d

ray structures of **2a**, **2d**, **2b**, and **2c**, respectively. In all of the complexes, two iron centers, each in a five-coordinate square-pyramidal geometry, are present in *anti* conformations. Except **2c**, which crystallizes in a triclinic crystal system with the $P\bar{1}$ space group, other molecules crystallize in the monoclinic crystal system with the $P2_1/c$ space group. Selected bond distances and angles are reported in Table 2. The packing diagrams of the complexes are shown in Figure 5 (for **2c**) and Figures S4–S6 (for complexes **2a**, **2b**, and **2d**, respectively). Figure 5 also reveals the intermolecular interaction between two thiophenolate rings (with an average distance of 3.41 Å) of the neighboring molecules. The thiophenolate rings are nearly cofacial to each other with a small offset favoring strong $\pi-\pi$ interaction.

The average Fe–Np bond distances for **2a**, **2b**, **2c**, and **2d** are 2.059(2), 2.052(4), 2.058(2), and 2.053(6)Å, respectively, which fall within the range observed for a high-spin ($S = 5/2$) Fe(III) porphyrin.[3,13] These values are comparable to the Fe–Np bond distance reported for axial thiophenolato coordination

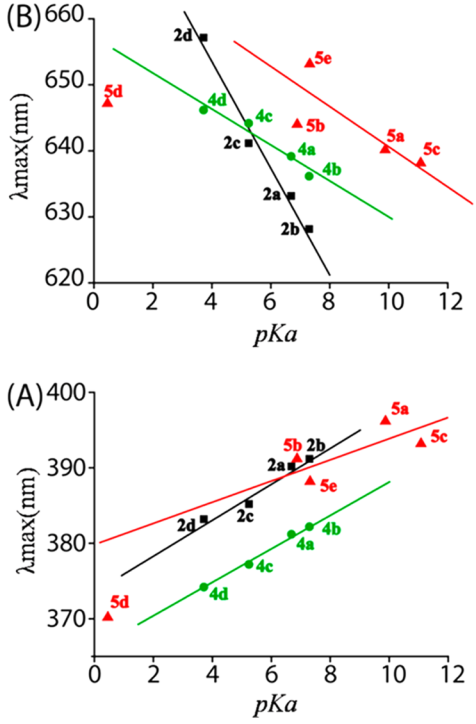

Figure 2. Correlation between pK_a values of conjugate acid of the thiophenols and phenols[3b] with the wavelength maxima of bisthiophenolatodiiron(III)bisporphyrins (■), bisphenolatodiiron-(III)bisporphyrins (▲), and thiophenolatoiron(III)monoporphyrins (●) for (A) Soret band and (B) band I.

to iron(III) monoporphyrins also.[8] For example, the reported Fe–Np bond distances for **4a**[8a] and $Fe^{III}(TPP)(SPh)\cdot C_6H_6$[8d] are 2.057 and 2.063 Å, respectively.

The Fe–S bond distances observed for **2a** and **2b** are 2.2829(11) and 2.2842(19) Å, respectively, while for **2c** and **2d**,

Table 1. UV–Visible Spectral Data of Complexes 2a–2d

thiophenols (complex)	pK_a	Soret band (nm)	band IV (nm)	band III (nm)	band I (nm)
thiophenol (**2a**)	6.61[a]	390	511	541	633
2,4,6-trimethylthiophenol (**2b**)	7.22[b]	391	514	546	628
2,6-dichlorothiophenol (**2c**)	5.17[b]	385	515	550	645
2,3,4,5,6-pentafluorothiophenol (**2d**)	3.64[b]	383	519	552	657

[a] pK_a was obtained from ref 11. [b] pK_a values were obtained from "calculated properties" for each compound in SciFinder.

dx.doi.org/10.1021/ic5011677 | *Inorg. Chem.* 2014, 53, 11925–11936

Chart 1

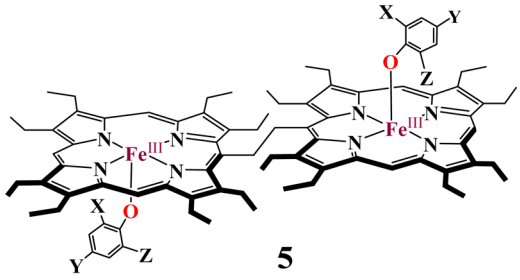

5

X	Y	Z	Complex
H	H	H	**5a**
Br	Br	Br	**5b**
^{i}Pr	H	^{i}Pr	**5c**
NO_2	NO_2	NO_2	**5d**
NO_2	H	H	**5e**

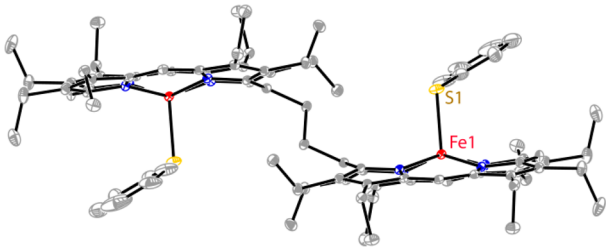

Figure 3. A perspective view of **2a** showing 50% thermal contours for all non-hydrogen atoms at 100 K (H atoms have been omitted for clarity).

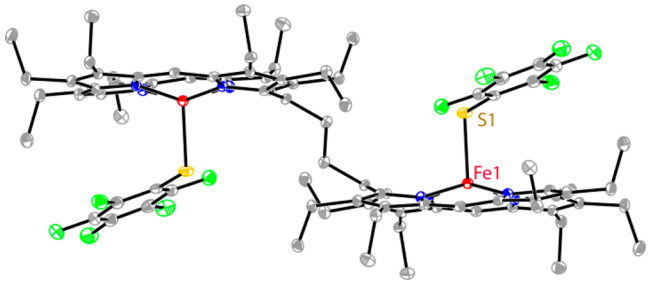

Figure 4. A perspective view of **2d** showing 50% thermal contours for all non-hydrogen atoms at 100 K (H atoms have been omitted for clarity).

Table 2. Selected Bond Distance (Å) and Angles (deg)

bond distances	2a	2b	2c	2d
Fe1−N1	2.064(2)	2.049(4)	2.052(2)	2.041(6)
Fe1−N2	2.054(2)	2.049(4)	2.055(2)	2.067(6)
Fe1−N3	2.062(2)	2.056(4)	2.062(2)	2.054(6)
Fe1−N4	2.057(2)	2.055(4)	2.062(2)	2.050(6)
Fe1−S1	2.2829(11)	2.2842(19)	2.3136(10)	2.316(2)
bond angles	2a	2b	2c	2d
N1−Fe1−N2	87.70(8)	88.05(16)	89.44(9)	88.1(2)
N1−Fe1−N3	150.02(9)	154.84(19)	155.87(9)	156.5(2)
N1−Fe1−N4	85.47(8)	85.31(17)	85.87(9)	85.8(2)
N2−Fe1−N3	86.09(8)	85.51(17)	86.09(9)	86.5(2)
N2−Fe1−N4	154.46(9)	151.2(2)	155.27(9)	152.2(3)
N3−Fe1−N4	87.63(8)	88.70(17)	88.35(9)	88.4(2)
Fe1−S1−C38	102.8513)	105.3(2)	101.27(10)	102.5(3)

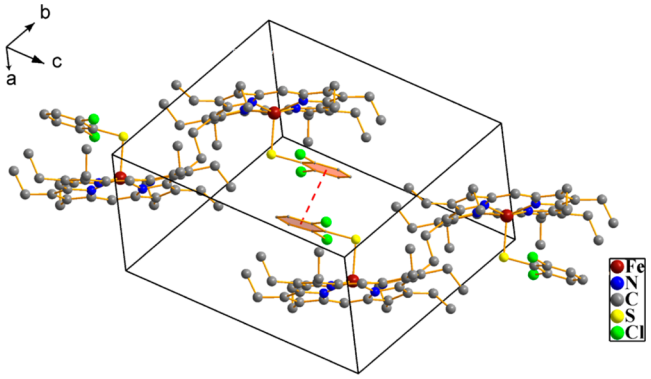

Figure 5. Diagram illustrating the packing of **2c** molecules in the unit cell and the $\pi-\pi$ interaction between the thiophenolate rings of two **2c** molecules (H atoms have been omitted for clarity).

the values are, respectively, 2.3136(10) and 2.316(2) Å. These values are comparable to the Fe−S bond distance reported so far for Fe(III)porphyrin with thiophenolato coordination.[8] For example, the reported Fe−S bond distances in **4a** and Fe^{III}(OEP)(S-2-$CF_3CONHC_6H_4$) are 2.299(3) and 2.327(4) Å, respectively.[8a,e,f] However, the Fe−S distance has been found to increase with increasing electron withdrawing substituents on the thiophenols, this is due to the fact that an electron withdrawing substituent with a strong −I effect reduces the electron donating ability of the iron bound sulfur atom and thereby increases the Fe−S bond length. The Fe−S−C bond angle for **2a** is 102.85(13)°, which is, however, identical to 102.5(3)°, observed in **4a**.[8a] The Fe−S−C angle for **2b** is 105.3(2)°, while for **2c** and **2d**, the angles are 101.27(10) and 102.5(3)°, respectively. As can be seen, the change in Fe−S−C angle is rather small in the series.

Five-coordinate iron(III) porphyrins are known to exist as high-spin (S = 5/2), intermediate-spin (S = 3/2), and also as a quantum mechanical spin admixed state with varying proportions of S = 3/2 and S = 5/2 states.[3,13−15] The structural parameters important for identifying the spin state of five-coordinate iron(III) porphyrins are the displacement of the iron from the mean plane of the $C_{20}N_4$ pophyrinato core (Fe···Ct_p) and the average Fe−Np distance.[3,13] For the high-spin case, the typical Fe−Np and Fe···Ct_p distances are ≥2.045 and ≥0.42 Å, respectively. On the other hand, values reported for five-coordinate spin-admixed iron(III) porphyrinates are in the range of 1.961−2.038 Å for Fe−Np and 0.10−0.36 Å for the displacements of the iron (Fe···Ct_p), varying according to the amount of S = 3/2 and 5/2 character present in the system. The average Fe−Np and Fe···Ct_p distances are 2.059(2) Å and 0.61 Å for **2a**, 2.052(4) Å and 0.58 Å for **2b**, 2.058(2) Å and 0.41 Å for **2c**, and 2.053(5) Å and 0.55 Å for **2d**, respectively, and the spin state can thus be assigned as a pure high-spin state of iron.

Table 3 compares the structural parameters of thiophenolato diiron(III)bisporphyrin complexes reported here along with their phenolato and monoporphyrin analogues. As can be seen, the average Fe−Np bond distances of the phenolato complexes **5a**−**5c** are in general greater than those of corresponding thiophenolato complexes **2a**−**2d**. The only exception being the case of **5d**,[3b] where the iron(III) center is in an intermediate-spin (S = 3/2) state resulting in a smaller Fe−Np distance. The Fe−S bond distances in **2a**−**2d** are larger compared to the Fe−O distances observed in their phenolato counterparts, **5a**−**5d**. This indicates that thiophenols are weaker donors than

dx.doi.org/10.1021/ic5011677 | Inorg. Chem. 2014, 53, 11925−11936

Table 3. Selected Structural Parameters for Five-Coordinate Fe^{III}(porphyrin)thiophenolate/phenolate Complexes

complex		$Fe-N_p$[a]	Fe−S/O[b] (L)	Fe−S/O−C[c]	Δ^{Fe}_{24}[d]	Δ_{24}[e]	C_m[f]	C_β[f]	Fe···Fe[g]	ref
2a		2.059(2)	2.2829(11)	102.85(13)	0.61	0.20	0.37	0.16	9.76	this work
2b		2.052(4)	2.2842(19)	105.3(2)	0.58	0.19	0.37	0.15	9.63	this work
2c		2.058(2)	2.3136(10)	101.27(10)	0.41	0.16	0.30	0.11	9.46	this work
2d		2.053(6)	2.316(2)	102.5(3)	0.55	0.19	0.35	0.15	9.75	this work
5a		2.057(3)	1.916(2)	134.4(2)	0.51	0.12	0.25	0.11	9.67	3b
5b		2.077(3)	1.864(3)	152.0(3)	0.52	0.08	0.07	0.13	10.09	3b
5c	core I	2.066(5)	1.807(4)	165.7(4)	0.55	0.20	0.40	0.15	9.94	3b
	core II	2.075(5)	1.813(4)	162.7(4)	0.56	0.13	0.24	0.11		
5d		1.972(3)	2.000(2)	127.2(2)	0.23	0.26	0.53	0.21	9.39	3b
Fe^{III}(OEP)(SPh)		2.057	2.299	102.51	0.51	0.07	0.12	0.07		8a
Fe^{III}(OEP){S-2,6-$(CF_3CONH)_2C_6H_3$}		2.048	2.356	104.55	0.48	0.05	0.06	0.06		8e
Fe^{III}(OEP)(S-2-$CF_3CONHC_6H_4$)		2.047	2.327	103.88	0.40	0.02	0.04	0.03		8e
Fe^{III}(TPP)(SPh)·C_6H_6		2.063	2.315	103.59	0.47	0.04	0.04	0.05		8d
Fe^{III}(TPP){S-2,6-$(CF_3CONH)_2C_6H_3$}·$1/2CH_2Cl_2$		2.042	2.333	105.86	0.47	0.27	0.02	0.53		8g
Fe^{III}(TPP)(S-2,3,5,6-$F_4C_6H_1$)		2.058	2.299	103.67	0.45	0.06	0.14	0.05		8g

[a]Average value in Å. [b]Distance (in Å) of axial ligand L. [c]Angle (in deg). [d]Displacement of iron from the least-squares plane of $C_{20}N_4$ porphyrinato core. [e]Average displacement of atoms from the least-squares plane of the $C_{20}N_4$ porphyrinato core. [f]Average displacement of the respective carbons from the mean plane of the $C_{20}N_4$ porphyrinato core. [g]Nonbonding distance (in Å) between two Fe(III) centers in a molecule.

phenols. The Fe−S−C angle in the complexes **2a**−**2d**, though much smaller than the Fe−O−C angles in the phenolato counterparts **5a**−**5d**,[3b] is similar to the Fe−S−C angles in the monoporphyrin complexes reported in the literature. The difference in the Fe−S/O−C bond angles as we shift from thiophenols to phenols are probably due to the shorter Fe−O distances compared to Fe−S distances. As the aromatic ring is drawn closer to the iron center, the steric interactions with the porphyrin ring increase, which subsequently increase the Fe−O−C angle in order to minimize the steric effect.

The porphyrin macrocycles are all distorted in the diiron(III)bisporphyrins reported in the present work in which the bridging *meso* carbons are displaced most. The core deformation of the thiophenolato complexes is similar to that observed in the case of their phenolato counterparts[3b] and is mostly ruffled. This can be best appreciated by turning to Figure 6, which compares the out-of-plane displacements in units of 0.01 Å of the porphyrin core atoms of **2a**−**2d**, **5a** (phenolato analog of **2a**), and **4a** (which is the monomeric analog of **2a**). While the porphyrin macrocycle in thiophenolato and phenolato complexes are highly distorted, the ring is planar in the related monomeric thiophenolato complex **4a**. As evident, the interaction between two rings in diheme results in larger ring deformation of the individual porphyrin centers. This has also been reflected in the average atom displacements from the mean porphyrin plane (Δ_{24}) and iron displacements therein (Δ^{Fe}_{24}), which are found to be 0.20 and 0.61 Å, respectively, for **2a** while for **4a** the values are 0.07 and 0.51 Å. It is also to be noted here that both the Δ_{24} and Δ^{Fe}_{24} are more in the thiophenolato complexes compared to the corresponding phenolato complexes of diiron(III)bisporphyrin.

Mössbauer. Mössbauer parameters are one of the most powerful probes to determine the spin states of the iron(III) porphyrins.[3,13] Figure 7 demonstrates the Mössbauer spectrum of the microcrystalline samples of **2a** at 298 K, which shows a small quadrupole splitting [δ (ΔEq): 0.28 (0.46) mm/s]

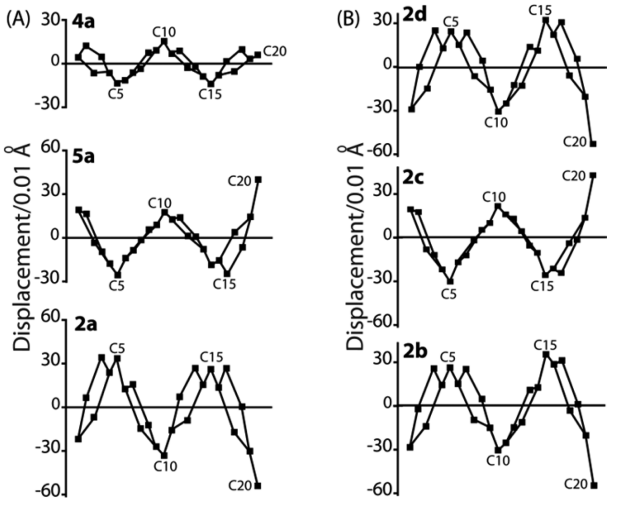

Figure 6. Atom deviations (in units of 0.01 Å) from the least-squares plane of the $C_{20}N_4$ porphyrinato core in (A) **2a**, **5a**,[3b] and **4a**[8a] and (B) **2b**, **2c**, and **2d**. The horizontal axis represents the atom number in the macrocycle (the numbering scheme is shown in Figure S7) showing the bond connectivity between atoms.

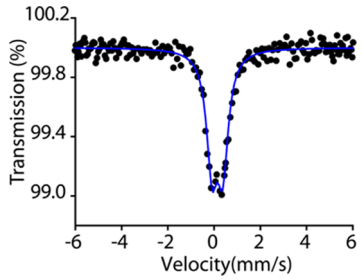

Figure 7. Zero-field Mössbauer spectra of microcrystalline samples of **2a** at 298 K.

dx.doi.org/10.1021/ic5011677 | Inorg. Chem. 2014, 53, 11925−11936

characteristic of the high-spin nature of Fe(III). Thus, Mössbauer parameters are consistent with the results obtained from the single-crystal X-ray structure of the complex (*vide supra*).

EPR. The EPR measurements were carried out at 120 K in both the solid and solution phases in dichloromethane, which show a similar spectral pattern for **2a** to **2d**; Figure 8 shows

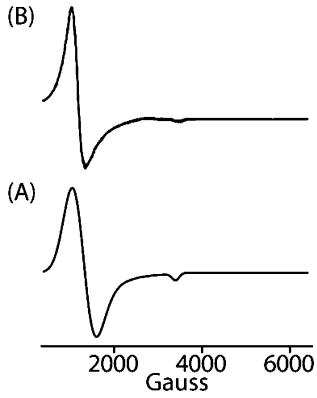

Figure 8. X-band EPR spectra in CH_2Cl_2 (at 120 K): (A) **2a** and (B) **2b**.

representative spectra of **2a** and **2b**, respectively. All the spectra are axially symmetric, and a careful simulation of these spectra (a representative simulated spectrum is shown in Figure S8) provided the following g values: $g_\perp = 5.95$ and $g_{II} = 2.00$ for **2a**, $g_\perp = 5.90$ and $g_{II} = 1.99$ for **2b**, $g_\perp = 5.90$ and $g_{II} = 2.00$ for **2c**, and $g_\perp = 5.85$ and $g_{II} = 2.00$ for **2d**. These results provide unequivocal evidence of the high-spin ($S = 5/2$) nature of the iron in the complexes in both the solid and solution phases.[3,13−15] The EPR spectra of the thiophenolato complexes **4a** to **4d** also bear the signature of a high-spin state in both a solid and solution under identical conditions.

However, the addition of excess thiophenol to the dichloromethane solution of **2** results in the formation of a six-coordinate low-spin complex **6** as depicted in Scheme 3. The UV−visible spectra of the pentacoordinate complex **2a** and the hexacoordinate complex **6a** are compared in Figure S9. A red shifting of the Soret band was observed upon formation of the hexacoordinate low-spin complex. The complexes **6a**−**6d** produce axial EPR spectra at 120 K typical for a low-spin state of iron which were then carefully simulated (a representative simulated spectrum is shown in Figure S10) to obtain the following g values: $g_\perp = 2.38$ and $g_{II} = 1.90$ for **6a**, $g_\perp = 2.42$ and $g_{II} = 1.85$ for **6b**, $g_\perp = 2.36$ and $g_{II} = 1.92$ for **6c**, and $g_\perp = 2.37$ and $g_{II} = 1.91$ for **6d**. Although no other structural data are available for the six-coordinate low-spin complex, it is expected that one axial ligand will bind as a thiophenolate, while the other one will bind as a thiophenol as also observed in the X-ray structure of $Fe^{III}(TPP)(C_6H_5S)(C_6H_5SH)$.[8h] Figure 9 compares the EPR spectra of **2a**, **6a**, and **6b** under identical conditions.

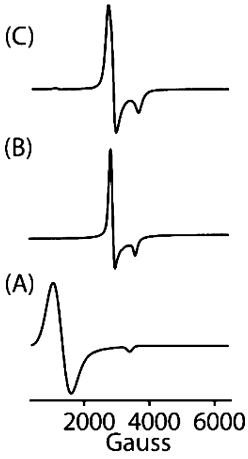

Figure 9. X-band EPR spectra in CH_2Cl_2 (at 120 K) (A) **2a**, (B) **6a**, and (C) **6b**.

Such conversion from the pentacoordinate high-spin Fe(III) complex to a hexacoordinate low-spin one is also observed in the case of cytochrome P-450. The addition of a water molecule at the vacant sixth coordination site of the cystine bound pentacoordinate high-spin iron(III) porphyrin of P-450 converts to hexacoordinated low-spin complex.[8h,16] It is to be noted that complete conversion to the low-spin complexes **6c** and **6d** was not achieved even after the addition of a large excess of corresponding thiophenols to **2c** and **2d**, respectively. A possible explanation could be the weakening of binding ability of the thiophenols with increasing acidity. However, in the case of the phenolato analogues **5a**−**5d**, the addition of a large excess of phenols did not produce any change in the EPR

Scheme 3

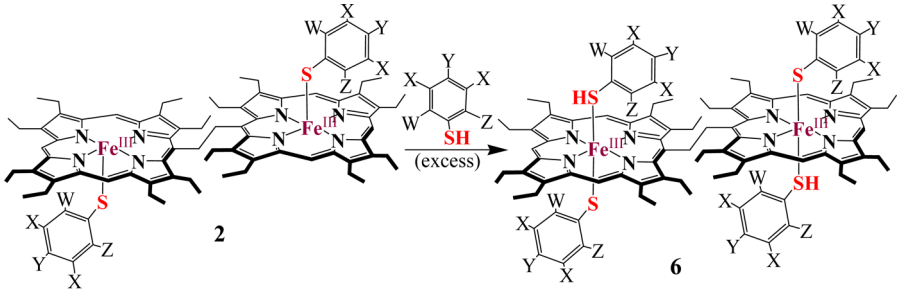

W	X	Y	Z	Complex
H	H	H	H	6a
Me	H	Me	Me	6b
Cl	H	H	Cl	6c
F	F	F	F	6d

dx.doi.org/10.1021/ic5011677 | *Inorg. Chem.* 2014, 53, 11925−11936

signal. Thus, the formation of the six-coordinate complex does not take place in solution in the case of the five-coordinate phenolato complexes.

^{1}H NMR. The structure and properties of the complexes in solution can be obtained from their ^{1}H NMR spectra in $CDCl_3$. The solid state structures are also preserved in solution as reflected in their ^{1}H NMR spectra. The signals are broad in general and shifted both upfield and downfield regions. The basic resonance pattern of porphyrin core for the thiophenolato complexes grossly resemble the pattern followed by *meso* substituted five-coordinate Fe(III) porphyrins of type XFe^{III}(*meso*-R-OEP).[3b] It is, therefore, expected that there should be two *meso*- resonances in 2:1 intensity ratio, eight methylene resonances, and four equally intense methyl resonances for a five-coordinate complex. The eight methylene resonances arise from the diastereotopic nature of these protons which occurs whenever the two sides of the porphyrin are inequivalent.

The ^{1}H NMR spectrum of **2a** is compared in Figure 10 with the previously reported complex of ethane-bridged diiron(III)-

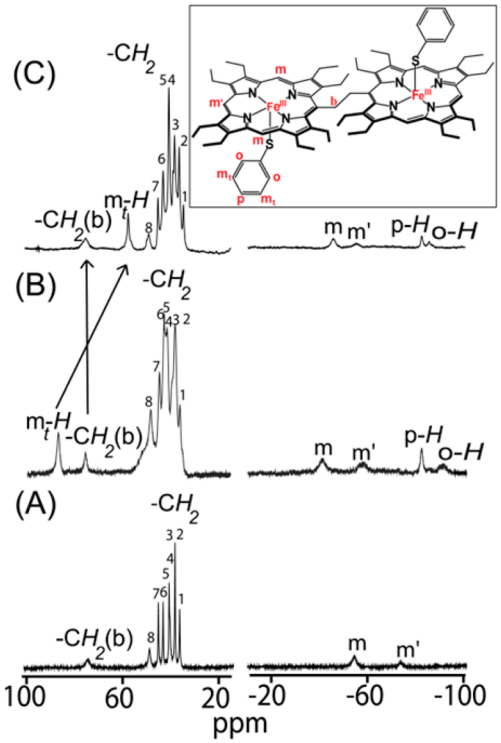

Figure 10. ^{1}H NMR spectra of (A) **7**,[3d] (B) **5a**,[3b] and (C) **2a** (inset shows the proton numbering scheme) in $CDCl_3$ at 295 K.

bisporphyrin with phenolate (**5a**)[3b] and chloride (**7** in Chart 2)[3d] axial ligands in which the spin state of iron was already

Chart 2

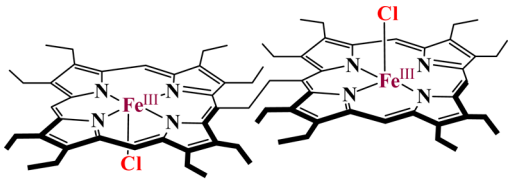

7

assigned as high-spin. For **2a**, eight diastereotopic methylene signals are observed at 33.5, 35.2, 37.1, 39.5, 41.9, 43.9, and 48.1 ppm; two *meso*- resonances are observed at −45.6 and −54.9 ppm in a 2:1 intensity ratio, while the bridging methylene signal is obtained at 72.5 ppm. Similarity in the nature and positioning of the ^{1}H NMR peaks with the chloride and phenolato complexes confirms the high-spin (S = 5/2) nature of iron in **2a** in solution as also observed in the solid (*vide supra*). Similar ^{1}H NMR spectra are also observed for other thiophenolato complexes (**2b**−**2d**) reported here and are compared in Figure 11. As can be seen, the nature and positions of methylene and *meso* protons bear the signature of a high-spin (S = 5/2) nature for all of the complexes.

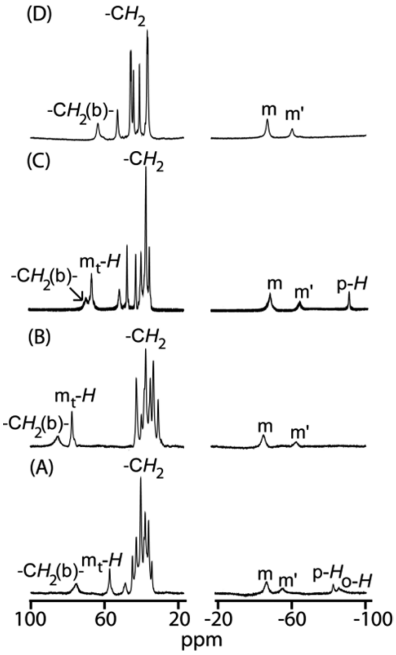

Figure 11. ^{1}H NMR spectra of (A) **2a**, (B) **2b**, (C) **2c**, and (D) **2d** in $CDCl_3$ at 295 K.

Chemical shifts of the CH_3 protons of the ethyl substituent are also known to be sensitive of spins. CH_3 signals of **2a** appear at 7.9 and 8.3 ppm. Methyl proton signals of **2b**−**2d** have also appeared in a similar spectral region. The downfield shifting of such resonances are due to delocalization of spin up to the CH_3 protons via σ bonds.[3b,17] Therefore, the positions of methyl resonances further support the spin state assignment for the complexes as shown above.

The thiophenolate resonances of **2** are, however, shifted to both upfield and downfield regions in the ^{1}H NMR as reflected in Figures 10 and 11, which indicate π-spin delocalization from the Fe(III) center to the thiophenolate ligand.[3a,b,e,9a] The *ortho* protons of the axial phenolate ligand are closest to the paramagnetic Fe center and have extremely small T_1 (spin−lattice relaxation) values resulting in a very broad signal at −85.9 ppm. The *meta* and *para* proton resonances are relatively sharp and are found at 56.4 and −82.7 ppm, respectively. In order to assign the peaks of the thiophenolate moiety successfully, various substituted thiophenols have been used here, and Figure 11 demonstrates the ^{1}H NMR spectra of **2a**−**2d**. As can be seen, the *ortho* and *para* protons show an upfield shift, while *meta* protons show a downfield one. Similar observations are also reported when substituted phenol and

dx.doi.org/10.1021/ic5011677 | *Inorg. Chem.* 2014, 53, 11925−11936

catechols are used as axial ligands.[3b,e,9,18] Figure S11 demonstrates the Mulliken spin densities, using DFT, of the thiophenolato carbons of **2a** in which spin densities are observed as positive at *ortho* and *para* positions and negative at the *meta* position. Therefore, the *ortho* and *para* protons should be shifted upfield, while the *meta* proton is in the downfield region, which is, however, observed in the ^{1}H NMR of the molecules. The alternating shift pattern, which is of the opposite sign of the chemical shifts for *meta* versus *ortho* and *para* protons, is also indicative of π-spin delocalization on the thiophenolato ligand.

The ^{1}H NMR spectra of the monoporphyrin counterpart **4a**−**4d** under identical conditions are presented in Figure S12. The ^{1}H NMR spectra of **4a** and **4b** in C_6D_6 were reported earlier.[8e] As displayed in Figure S12, two methylene and one *meso* proton signal are observed in the complexes, which is, however, expected for the five-coordinate complex. The two methylene resonances arise from the diastereotopic nature of these protons, which occurs whenever the two sides of the porphyrin are inequivalent due to axial coordination. The *ortho* and *para* protons of the thiophenolate are upfield shifted, while the *meta* proton is downfield shifted, as seen in the case of diheme analogues **2a**−**2d**.

Cyclic Voltammetry. Cyclic voltammetry was performed at 298 K under N_2 in CH_2Cl_2 using 0.1 M tetra(*n*-butyl)-ammonium hexafluorophosphate (TBAH) as the supporting electrolyte. The Fe(III)/Fe(II) redox potential of **2a**, **2b**, **2c**, and **2d** are observed at −0.76, −0.90, −0.54, and −0.36 V vs Ag/AgCl, respectively, and three representative spectra have been shown in Figure 12. The Fe(III)/Fe(II) redox potentials

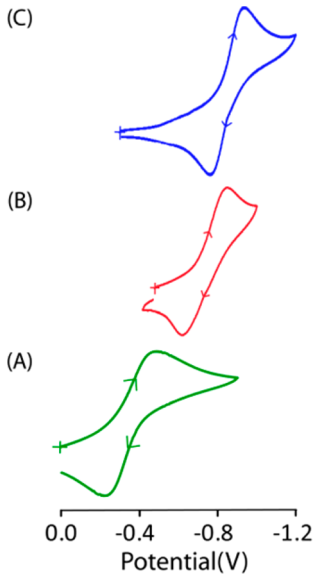

Figure 12. A portion of the cyclic voltammograms of (A) **2e**, (B) **2a**, and (C) **2b** at 298 K in CH_2Cl_2 (scan rate 100 mV/s) with 0.1 M tetra(*n*-butyl)ammonium hexafluorophosphate as a supporting electrolyte. The reference electrode was Ag/AgCl.

of **4b**, **4c**, and **4d** have also been measured and are listed in the Experimental Section, while that of **4a** (−0.68 V vs SCE in dichloromethane) has been obtained from the literature.[8f] The redox potentials of native cytochrome P-450$_{cam}$ were reported to be −0.415 V vs SCE for substrate binding mode and −0.572 V vs SCE for nonsubstrate binding mode.[8e,i] The positively shifted redox potential of **2c** (−0.584 V vs SCE) is close to that of substrate-free cytochrome P-450$_{cam}$.

Coulometric reduction of the thiophenolato complexes in dichloromethane at a constant potential has also been performed, and the progress of the reaction was monitored continuously by UV−visible spectroscopy as shown in Figure S13 for **2c**, as a representative case. A gradual decrease of Soret band characteristics of Fe(III)porphyrin and the appearance of a new Soret band corresponding to Fe(II) confirms the corresponding potential as that of the Fe(III)/Fe(II) redox couple.[19] The positively shifted Fe(III)/Fe(II) redox couple of complex **2a** ($E_{1/2}$ = −0.76 V) compared to that of phenolato complex **5a** ($E_{1/2}$ = −0.92 V) suggests that thiophenol is a weaker electron donor than phenol, which is due to back-donation of electron density from the iron center to an empty d orbital of sulfur. Since oxygen does not have a low-lying 3d orbital, similar back-donation of the electron from iron to oxygen is not possible with phenol. Therefore, the electron density of iron in **2a** should be lower than that in **5a**, which explains why the iron center of the former complex is more reducible.

For complex **7**[3d] and complexes **5a**−**5e**,[3b] it has been observed that on moving from monoheme to diheme, the Fe(III)/Fe(II) redox potential is shifted toward the more negative value. For complexes **2a**−**2d**, however, such a trend has not been observed. With thiophenol having a lower pK_a, the Fe(III)/Fe(II) potential of the diheme was found to follow the reverse trend, i.e., more positively shifted compared to its monoheme analogues. Thus, the pK_a of the coordinated thiophenols plays a crucial role in deciding the nature of shift of the Fe(III)/Fe(II) redox couple.

A plot of Fe(III)/Fe(II) potential of **2a**−**2d** against pK_a of the thiophenols is shown in Figure 13, in which a linear

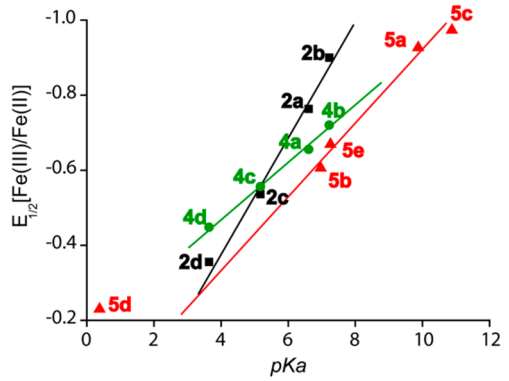

Figure 13. Plots of pK_a of thiophenols/phenols vs $E_{1/2}$ [Fe(III)/Fe(II)] in V of bisthiophenolatodiiron(III)bisporphyrins (■), bisphenolatodiiron(III)biporphyrins (▲), and thiophenolatoiron(III)-monoporphyrins (●).

relationship has been observed. Such linear relationships have also been obtained for the monomeric counterpart **4a**−**4d**. The electrochemical data suggest that the thiophenolato complex with a more acidic thiophenol has a more positively shifted Fe(III)/Fe(II) couple. Increasing the number of electron withdrawing substituents on the thiophenol ring increases its acidity and thus shifts the Fe(III)/Fe(II) redox potential more toward positive, while the electron donating substituent leads to an opposite effect. A similar pK_a dependence of the Fe(III)/Fe(II) redox couple has been obtained (Figure 13) for the

dx.doi.org/10.1021/ic5011677 | Inorg. Chem. 2014, 53, 11925−11936

phenolato analogues **5a**−**5e** also;[3b] a deviation from linearity has been observed for **5d** due to a change of metal spin.

Shifting of the Fe(III)/Fe(II) redox couple is, however, known in the literature;[8] for example, in the case of Fe^{III}(TPP){S-2,6-$(CF_3CONH)_2C_6H_3$}, Fe^{III}(OEP)(S-2-$CF_3CONHC_6H_4$), Fe^{III}(OEP){S-2,6-$(CF_3CONH)_2C_6H_3$}, Fe^{III}(OEP)(S-2-$CF_3CONHC_6H_4$), and **4a**, the Fe(III)/Fe(II) redox potentials are −0.19, −0.41, −0.25, −0.52, and −0.68 V respectively vs SCE in dichloromethane.[8b,f,g] The variation in the Fe(III)/Fe(II) redox potential has been suggested as a result of a hydrogen bond (NH····S) while the electronic effect by *ortho* and *para* substituent on the thiophenol was found to be insignificant.[8b,f] Among complexes of Fe^{III}(OEP){S-2,6-$(CF_3CONH)_2C_6H_3$}, Fe^{III}(OEP)(S-2-$CF_3CONHC_6H_4$), and **4a**, a variation of 430 mV in the Fe(III)/Fe(II) couple was obtained by the influence of intramolecular NH····S hydrogen bonding.[8b,f] In the present investigation, however, the effect of substituent on the thiophenol ring toward the Fe(III)/Fe(II) redox potential has been explored varying the substituent from electron donating (**2b**) to electron withdrawing (**2c**, **2d**). Modulating electronic property of the substituent leads to a wide potential window of 540 mV for Fe(III)/Fe(II) redox couple in the series **2a**−**2d**. However, in the case of monomeric analogues **4a**−**4d**, the variation in Fe(III)/Fe(II) redox potential on varying such electronic properties of thiophenols is only 270 mV, which is half of the potential range observed in diheme. Such an increase in the potential range on going from monoheme to diheme can be attributed as a result of heme−heme interaction present in dihemes.

Cyclic voltammogram of the six-coordinate complex **6a** has also been measured under identical conditions, in which the Fe(III)/Fe(II) redox couple was observed at −0.27 V (versus Ag/AgCl). The large positive shift of 490 mV in the Fe(III)/Fe(II) redox potential of **6a**, as compared to **2a**, suggests that the reduction of the iron center becomes much easier upon coordination of an extra thiophenol at the sixth position which eventually leads to changing the metal spin from high to low. Figure 14 compares the cyclic voltammograms of both five- (**2a**) and six-coordinate complexes (**6a**). Such a positive shift in the Fe(III)/Fe(II) redox potential can be attributed to the contributions from the sixth axial coordination as well as a change of metal spin (from high to low-spin). Earlier, it was demonstrated that the change in the spin state of the Fe(III) center is found to significantly influence the Fe(III)/Fe(II) redox potential.[3b] The control of heme redox potential by controlling the spin state is crucial for the functioning of cytochrome P450.[8h,k]

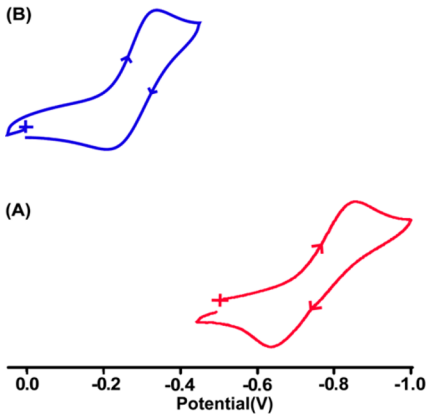

Figure 14. A portion of the cyclic voltammograms of (A) **2a** and (B) **6a** at 298 K in CH_2Cl_2 (scan rate 100 mV/s) with 0.1 M tetra(*n*-butyl)ammonium hexafluorophosphate as the supporting electrolyte. The reference electrode was Ag/AgCl.

Computational Studies. Density functional calculations have been carried out using the B3LYP hybrid functional[20−22] using the Gaussian 03, revision B.04, package.[23] The single point energy calculations were performed for **2a**, **5a**, and **7** using the LANL2DZ basis set for iron atoms and the 6-31G** basis set for all other atoms. Atom coordinates of **2a** and **5a** have been obtained from the respective crystal structures while geometry optimization of **7** has been performed with the help of DFT. Figure 15 represents a qualitative plot of the relative

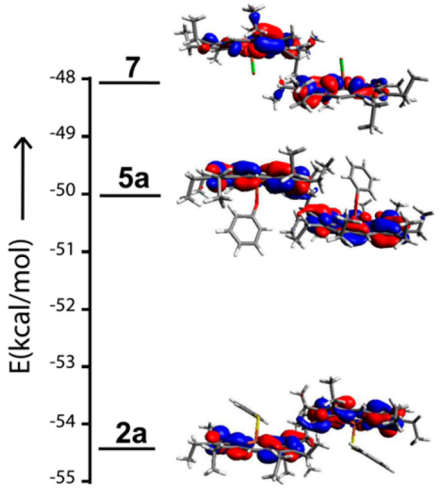

Figure 15. A plot showing the relative energies of the LUMOs for **2a**, **5a**, and **7**.

energy of LUMOs for **2a**, **5a**, and **7**. Reduction of metalloporphyrin systems can be seen as an addition of electrons to the LUMO; therefore, a compound with a low energy LUMO will be easier to reduce. The LUMO of **2a** was found to be lowest in energy and that of **7** being highest with **5a** in between. This explains the positive shifting of the Fe(III)/Fe(II) couple as we move from **7** to **5a** to **2a**, which also supports our experimental observation. As can be seen in Figure 16, the

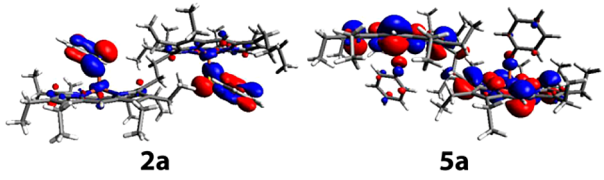

Figure 16. A plot showing the HOMOs for (A) **2a** and (B) **5a**.

HOMO is more localized on the thiophenolate ligand with significant amplitude on the sulfur atom in **2a**, while it is more localized on the porphyrin ring in **5a**, which suggests the back-donation of an electron in the thiophenolato complex.

■ CONCLUSIONS

Syntheses, structure, and properties of a series of diiron(III)-bisporphyrins with axial thiophenolate coordination have been reported. The porphyrin macrocycle in the diheme complexes is found to be more distorted compared to the monoheme analogues. Electrochemical data reveal a good linear relation-

dx.doi.org/10.1021/ic5011677 | *Inorg. Chem.* 2014, 53, 11925−11936

ship between the Fe(III)/Fe(II) redox couple and pK_a of thiophenol. The Fe(III)/Fe(II) redox couple has been shifted more positively in the thiophenolato complex compared to their phenolato analogue due to the presence of low-lying vacant 3d orbitals in sulfur which facilitates the back-donation of an electron from the iron center. Changing the electronic nature of the substituents on the thiophenolate ring in diheme has been found to change the Fe(III)/Fe(II) redox potential up to 540 mV (in contrast to the value of only 270 mV in case of monoheme analogues). The pK_a of the coordinated thiophenol has been found to play a crucial role in deciding the nature of the shift of the Fe(III)/Fe(II) redox couple, while the inter-ring interaction decides the extent of shifting. The large difference in structural, chemical, and electrochemical properties of the diheme as compared to the monoheme analog provide unequivocal evidence of the role played by heme−heme interaction in diheme.

Additions of excess thiophenol to the dichloromethane solution of five-coordinate thiophenolate complex results in the formation of a six-coordinate low-spin complex which shows a large positive shift of 0.49 V in the Fe(III)/Fe(II) redox couple. Such a large positive shift is attributed to the contributions from the sixth axial coordination as well as change of iron spin (from high to low).

EXPERIMENTAL SECTION

Materials. μ-Oxo-syn-1,2-bis[5-(2,3,7,8,12,13,17,18-octaethylporphyrinato)iron(III)]ethane, **1**; μ-oxo-bis-[(2,3,7,8,12,13,17,18-octaethylporphyrinato)iron(III)], **3**; (thiophenolato)(2,3,7,8,12,13,17,18-octaethylporphyrinato)iron(III), **4a**; (2,4,6-trimethylthiophenolato)(2,3,7,8,12,13,17,18-octaethylporphyrinato)iron(III), **4b**; and 1,2-bis[(chloro){5-(2,3,7,8,12,13,17,18-octaethylporphyrinato)}iron(III)]ethane, **7**, were prepared using the methods reported earlier.[8b,3c,16,24] Reagents and solvents were purchased from commercial sources and purified by standard procedures before use.

Synthesis. Complexes **2a**−**2d** were prepared using the general procedure; details for one representative case have been described below.

Syntheses of ***2a***. A total of 100 mg of **1** (0.082 mmol) was dissolved in 100 mL of dichloromethane, and thiophenol (18.07 mg, 0.164 mmol) was added to it. The mixture was then stirred for 30 min under nitrogen. During the progress of the reaction, the green solution changed to bright red, and the resulting solution was then evaporated to complete dryness. The solid thus obtained was then dissolved in a minimum volume of benzene and carefully layered with *n*-hexane. On standing for 6−8 days in air at room temperature, a dark purple crystalline solid was formed, which was collected by filtration, washed well with the mother liquor, and dried in a vacuum. Yield: 88 mg (76%). Anal. Calcd (found): C, 72.60 (72.79); H, 7.09 (7.35); N, 7.88 (7.91). UV−vis (dichloromethane) [λ_{max}, nm (ε, M^{-1} cm^{-1})]: 390 (1.2×10^5), 413 (1.05×10^5), 511 (2.52×10^4), 541 (2.45×10^4) 633 (1.95×10^4). ^{1}H NMR ($CDCl_3$, 295 K) *meso-H*: −45.6, −54.9; CH_3: 7.9, 8.3; CH_2: 33.5, 35.2, 37.1, 39.5, 41.9, 43.9, 48.1; CH_2(b): 72.5. *o-H*: −85.9; *p-H*: −82.7; m_t-*H*: 56.4 ppm. $E_{1/2}$ (Fe^{3+}/Fe^{2+}), V: −0.76.

2b. Yield: 90 mg (73%). Anal. Calcd (found): C, 73.38 (73.55); H, 7.50 (7.84); N, 7.44 (7.48). UV−vis (dichloromethane) [λ_{max}, nm (ε, M^{-1} cm^{-1})]: 391 (1.46×10^5), 415 (1.3×10^5), 514 (2.6×10^4), 546 (2.51×10^4) 628 (1.91×10^4). ^{1}H NMR ($CDCl_3$, 295 K) *meso-H*: −44.9, −62.6; CH_3: 7.3, 7.4; CH_2: 30.9, 33.7, 35.1, 37.6, 38.4, 42.7; CH_2(b): 85.4; m_t-*H*: 77.7 ppm. $E_{1/2}$ (Fe^{3+}/Fe^{2+}), V: −0.90.

2c. Yield: 110 mg (86%). Anal. Calcd (found): C, 66.24 (66.49); H, 6.21 (6.60); N, 7.19 (7.22). UV−vis (dichloromethane) [λ_{max}, nm (ε, M^{-1} cm^{-1})]: 385 (1.37×10^5), 410 (1.12×10^5), 515 (1.98×10^4), 550 (1.75×10^4), 645 (1.62×10^4). ^{1}H NMR ($CDCl_3$, 295 K) *meso-H*: −47.9, −64.2; CH_3: 7.7, 7.9; CH_2: 35.5, 37.4, 40.1, 42.9, 47.6, 51.8; CH_2(b): 69.6. *p-H*: −90.5; m_t-*H*: 66.7 ppm. $E_{1/2}$ (Fe^{3+}/Fe^{2+}), V: −0.54.

2d. Yield: 98 mg (75%). Anal. Calcd (found): C, 64.50 (64.33); H, 5.66 (5.75); N, 7.00 (7.15). UV−vis (dichloromethane) [λ_{max}, nm (ε, M^{-1} cm^{-1})]: 383 (1.28×10^5), 418 (1.06×10^5), 519 (1.85×10^4), 552 (1.70×10^4) 657 (1.58×10^4).^{1}H NMR ($CDCl_3$, 295 K) *meso-H*: −46.7, −60.2; CH_3: 7.5, 7.9, 8.2; CH_2: 36.5, 36.9, 41.1, 44.3, 45.6, 46.1; CH_2(b): 63.6 ppm. $E_{1/2}$ (Fe^{3+}/Fe^{2+}), V: −0.36.

4b. UV−vis (dichloromethane) [λ_{max}, nm (ε, M^{-1} cm^{-1})]: 382 (9.1×10^4), 504 (1.2×10^3), 533 (1.0×10^3), 632 (7.8×10^2). $E_{1/2}$ (Fe^{3+}/Fe^{2+}), V: −0.72.

4c. Yield: 95 mg (74%). Anal. Calcd (found): C, 65.80 (65.63); H, 6.18 (6.27); N, 7.31(7.25). UV−vis (dichloromethane) [λ_{max}, nm (ε, M^{-1} cm^{-1})]: 377 (1.3×10^5), 514 (6.1×10^3), 534 (5.8×10^3), 643 (9.8×10^2). ^{1}H NMR ($CDCl_3$, 295 K) *meso-H*: −48.7; CH_3: 8.8; CH_2: 40.1, 46.9; *p-H*: −90.2; m_t-*H*: 67.3 ppm. $E_{1/2}$ (Fe^{3+}/Fe^{2+}), V: −0.56.

4d. Yield: 99 mg (75%). Anal. Calcd (found): C, 64.04 (64.15); H, 5.63 (5.75); N, 7.11 (7.03). UV−vis (dichloromethane) [λ_{max}, nm (ε, M^{-1} cm^{-1})]: 374 (1.54×10^5), 510 (7.8×10^3), 534 (6.5×10^3), 647 (1.2×10^3). ^{1}H NMR ($CDCl_3$, 295 K) *meso-H*: −47.9; CH_3: 7.6, 7.3; CH_2: 42.0, 47.9 ppm. $E_{1/2}$ (Fe^{3+}/Fe^{2+}), V: −0.45.

Theoretical Calculation. DFT calculations have been carried out by employing a B3LYP[20−22] hybrid functional using the Gaussian 03, revision B.04, package.[23] The method used was Becke's three parameter hybrid exchange functional; the nonlocal correlation provided by the Lee, Yang, and Parr expression; and Vosko, Wilk, and Nuair 1980 correlation functional (III) for local correction.[20−22] The basis set was LanL2DZ for the iron atom and 6-31G** for carbon, nitrogen, sulfur, oxygen, and hydrogen atoms. All the calculations were performed with a multiplicity of 11, and no structural relaxations were carried out. Atom coordinates of **2a** and **5a**[3b] have been obtained from the respective crystal structures. In the absence of X-ray structure, geometry optimization of **7** has been performed with the help of DFT using the initial atom coordinates from the X-ray structure of *trans*-1,2-*bis*[chloroiron(III)5-(2,3,7,8,12,13,17,18-octaethylporphyrinyl)]-ethene.[3e] Visualization of the molecular orbitals and the corresponding diagrams were made using the Avogadro software.[25]

Instrumentation. UV−vis spectra were recorded on a PerkinElmer UV/vis spectrometer. Electron paramagnetic resonance (EPR) spectra were obtained on a Bruker EMX EPR spectrometer. Elemental (C, H, and N) analyses were performed on a PerkinElmer 2400II elemental analyzer. ^{1}H NMR spectra were recorded on a JEOL 500 MHz instrument. The spectra for paramagnetic molecules were recorded over a 100-kHz bandwidth with 64 K data points and a 5 ms 90° pulse. For a typical spectrum, between 2000 and 3000 transients were accumulated with a 50-μs delay time. The residual ^{1}H resonances of the solvents were used as a secondary reference. Cyclic voltammetric studies were performed on a BAS Epsilon electrochemical workstation in dichloromethane with 0.1 M tetrabutylammonium hexafluorophoshate (TBAH) as a supporting electrolyte, and the reference electrode was Ag/AgCl and the auxiliary electrode was a Pt wire. The concentration of the compounds was on the order of 10^{-3} M. The ferrocene/ferrocenium couple occurs at $E_{1/2}$ = +0.45 (65) V versus Ag/AgCl under the same experimental conditions. ^{57}Fe Mössbauer spectra were recorded using a Wissel 1200 spectrometer and a proportional counter. ^{57}Co(Rh) in a constant acceleration mode was used as the radioactive source. Isomer shifts (δ) are given related to α-iron foil at room temperature.

X-ray Structure Solution and Refinement. Single-crystal X-ray data were collected at 100 K on a Bruker SMART APEX CCD diffractometer equipped with CRYO Industries low-temperature apparatus, and intensity data were collected using graphite-monochromated Mo Kα radiation (λ = 0.71073 Å). The data integration and reduction were processed with SAINT software.[26] An absorption correction was applied.[27] The structure was solved with the direct method using SHELXS-97 and was refined on F^2 by full-matrix least-squares technique using the SHELXL-97 program package.[28] Non-hydrogen atoms were refined anisotropically. The hydrogen atoms were included in calculated positions. In the refinement, hydrogens were treated as riding atoms using SHELXL default

dx.doi.org/10.1021/ic5011677 | Inorg. Chem. 2014, 53, 11925−11936

Table 4. Crystal Data and Data Collection Parameters

	2a	2b	2c	2d
formula	$C_{86}H_{100}Fe_2N_8S_2$	$C_{92}H_{112}Fe_2N_8S_2$	$C_{86}H_{96}Cl_4Fe_2N_8S_2$	$C_{86}H_{90}F_{10}Fe_2N_8S_2$
T, K	100(2)	100(2)	100(2)	100(2)
fw	1421.56	1505.72	1559.33	1601.48
cryst syst	monoclinic	monoclinic	triclinic	monoclinic
space group	$P2_1/c$	$P2_1/c$	$P\bar{1}$	$P2_1/c$
a, Å	14.517(5)	14.850(5)	11.627(5)	14.647(5)
b, Å	17.068(5)	17.254(5)	12.813(5)	17.029(5)
c, Å	14.872(5)	15.114(5)	14.097(5)	14.927(5)
α, deg	90.000(5)	90.000(5)	67.275(5)	90.000(5)
β, deg	90.352(5)	93.611(5)	73.455(5)	91.512(5)
γ, deg	90.000(5)	90.000(5)	84.451(5)	90.000(5)
V, Å^3	3685(2)	3865(2)	1856.7(13)	3722(2)
radiation (λ, Å)	Mo Kα (0.71073)	Mo Kα (0.71073)	Mo Kα (0.71073)	Mo Kα (0.71073)
Z	2	2	1	2
d_{calcd}, g cm^{-3}	1.281	1.294	1.395	1.429
$F(000)$	1512	1608	820	1672
μ, mm^{-1}	0.502	0.483	0.644	0.525
no. of unique data	6834	7162	6864	6848
no. of params refined	450	480	468	495
GOF on F^2	1.031	1.051	1.027	1.067
$R1^a$ [$I > 2\sigma(I)$]	0.0479	0.0840	0.0465	0.1096
$R1^a$ (all data)	0.0646	0.1343	0.0673	0.1434
$wR2^b$ (all data)	0.1270	0.2376	0.1182	0.3302
largest diff. peak and hole	1.019 and −0.383 e.Å^{-3}	0.854 and −0.463 e.Å^{-3}	0.509 and −0.296 e.Å^{-3}	2.742 and −0.648 e.Å^{-3}

$^aR1 = \frac{\sum ||F_o|-|F_c||}{\sum |F_o|}$ $^bwR2 = \sqrt{\frac{\sum[w(F_o^2-F_c^2)^2]}{\sum[w(F_o^2)^2]}}$

parameters. Crystallographic data and data collection parameters are given in Table 4.

■ ASSOCIATED CONTENT

Supporting Information

UV−visible spectral change upon gradual addition of thiophenol to a dichloromethane solution of **1** (Figure S1); X-ray structures of **2b** and **2c** (Figures S2 and S3); packing diagrams of **2a**, **2b**, and **2d** (Figures S4−S6); atom numbering scheme used for out-of-plane displacement plots (Figure S7); experimental and simulated EPR spectra of **2b** (Figure S8); UV−visible spectra of **2a** and **6a** in dichloromethane (Figure S9); experimental and simulated EPR spectra of **6b** (Figure S10); Mulliken spin density plots for **2a** (Figure S11); ^{1}H NMR spectra of complexes **4a**−**4d** (Figure S12); UV−visible spectral change upon one-electron reduction of **2e** (Figure S13). X-ray crystallographic details in CIF format. This material is available free of charge via the Internet at http://pubs.acs.org.

■ AUTHOR INFORMATION

Corresponding Author

*E-mail: sprath@iitk.ac.in.

Notes

The authors declare no competing financial interest.

■ ACKNOWLEDGMENTS

The authors thank Science and Engineering Research Board (SERB), New Delhi and CSIR, New Delhi for financial support. D.S. and F.S.T.K. thank UGC, India for their fellowship.

■ DEDICATION

Dedicated to Professor Marilyn M. Olmstead on the occassion of her 70th birthday.

■ REFERENCES

(1) (a) Mayfield, J. A.; Dehner, C. A.; DuBois, J. L. *Curr. Opin. Chem. Biol.* **2011**, *15*, 260. (b) Fonseca, B. M.; Paquete, C. M.; Salgueiro, C. A.; Louro, R. O. *FEBS Lett.* **2012**, *586*, 504. (c) Paquete, C. M.; Louro, R. O. *Dalton Trans.* **2010**, *39*, 4259. (d) Akutsu, H.; Takayama, Y. *Acc. Chem. Res.* **2007**, *40*, 171. (e) Louro, R. O. *J. Biol. Inorg. Chem.* **2007**, *12*, 1. (f) Stevens, J. M.; Daltrop, O.; Allen, J. W. A.; Ferguson, S. J. *Acc. Chem. Res.* **2004**, *37*, 999. (g) Leys, D.; Meyer, T. E.; Tsapin, A. S.; Nealson, K. H.; Cusanovich, M. A.; Van Beeumen, J. J. *J. Biol. Chem.* **2002**, *277*, 35703. (h) Czjzek, M.; ElAntak, L.; Zamboni, V.; Morelli, X.; Dolla, A.; Guerlesquin, F.; Bruschi, M. *Structure* **2002**, *10*, 1677.

(2) Heitmann, D.; Einsle, O. *Biochemistry* **2005**, *44*, 12411.

(3) (a) Bhowmik, S.; Ghosh, S. K.; Rath, S. P. *Chem. Commun.* **2011**, *47*, 4790. (b) Bhowmik, S.; Dey, S.; Sahoo, D.; Rath, S. P. *Chem.—Eur. J.* **2013**, *19*, 13732. (c) Ghosh, S. K.; Patra, R.; Rath, S. P. *Inorg. Chem.* **2008**, *47*, 10196. (d) Ghosh, S. K.; Patra, R.; Rath, S. P. *Inorg. Chem.* **2010**, *49*, 3449. (e) Bhowmik, S.; Sil, D.; Patra, R.; Rath, S. P. *J. Chem. Sci.* **2011**, *123*, 827. (f) Ghosh, S. K.; Patra, R.; Rath, S. P. *Inorg. Chim. Acta* **2010**, *363*, 2791. (g) Bhowmik, S.; Ghosh, S. K.; Layek, S.; Verma, H. C.; Rath, S. P. *Chem.—Eur. J.* **2012**, *18*, 13025. (h) Ghosh, S. K.; Rath, S. P. *J. Am. Chem. Soc.* **2010**, *132*, 17983. (i) Ghosh, S. K.; Bhowmik, S.; Sil, D.; Rath, S. P. *Chem.—Eur. J.* **2013**, *19*, 17846.

(4) (a) Liu, J.; Chakraborty, S.; Hosseinzadeh, P.; Yu, Y.; Tian, S.; Petrik, I.; Bhagi, A.; Lu, Y. *Chem. Rev.* **2014**, *114*, 4366. (b) Barker, P. D.; Ferguson, S. J. *Structure* **1999**, *7*, R281.

(5) Rodrigues, M. L.; Oliveira, T. F.; Pereira, I. AC.; Archer, M. *EMBO J.* **2006**, *25*, 5951.

(6) (a) McRee, D. E.; Williams, P. A.; Sridhar, V.; Pastuszyn, A.; Bren, K. L.; Patel, K. M.; Chen, Y.; Todaro, T. R.; Sanders, D.; Luna, E.; Fee, J. A. *J. Biol. Chem.* **2001**, *276*, 6537. (b) Echalier, A.; Goodhew, C. F.; Pettigrew, G. W.; Fülöp, V. *Structure* **2006**, *14*, 107. (c) Pokkuluri, P. R.; Londer, Y. Y.; Duke, N. E. C.; Erickson, J.; Pessanha, M.; Salgueiro, C. A.; Schiffer, M. *Protein Sci.* **2004**, *13*, 1684. (d) George, G. N.; Richards, T.; Bare, R. E.; Gea, Y.; Prince, R. C.; Stiefel, E. I.; Watt, G. D. *J. Am. Chem. Soc.* **1993**, *115*, 7716.

(7) (a) Ortiz de Montellano, P. R. *Cytochrome P450: structure, mechanism and biochemistry*, 3rd ed.; Plenum, Kluwer: New York, 2005. (b) Dawson, J. H.; Sono, M. *Chem. Rev.* **1987**, *87*, 1255. (c) Dawson, J. H. *Science* **1988**, *240*, 433. (d) Higuchi, T.; Uzu, S.; Hirobe, M. *J. Am. Chem. Soc.* **1990**, *112*, 7051. (e) Mansuy, D. *Pure Appl. Chem.* **1987**, *59*, 759.
(8) (a) Miller, K. M.; Strouse, C. E. *Acta. Crystallogr., Sect. C* **1991**, *113*, 2501. (b) Uno, T.; Hatano, K.; Nishimura, Y.; Arata, Y. *Inorg. Chem.* **1990**, *29*, 2803. (c) de Visser, S. P.; Shaik, S.; Sharma, P. K.; Kumar, D.; Thiel, W. *J. Am. Chem. Soc.* **2003**, *125*, 15779. (d) Byrn, M. P.; Strouse, C. E. *J. Am. Chem. Soc.* **1991**, *113*, 2501. (e) Ueyama, N.; Nishikawa, N.; Yamada, Y.; Okamura, T.; Oka, S.; Sakurai, H.; Nakamura, A. *Inorg. Chem.* **1998**, *37*, 2415. (f) Ueyama, N.; Nishikawa, N.; Yamada, Y.; Okamura, T.; Nakamura, A. *J. Am. Chem. Soc.* **1996**, *118*, 12826. (g) Ueyama, N.; Nishikawa, N.; Yamada, Y.; Okamura, T.; Nakamura, A. *lnorg. Chim. Acta.* **1998**, *283*, 91. (h) Collman, J. P.; Sorrell, T. N.; Hodgson, K. O.; Kulshrestha, A. K.; Strouse, C. E. *J. Am. Chem. Soc.* **1977**, *99*, 5180. (i) Fisher, M. T.; Sligar, S. G. *J. Am. Chem. Soc.* **1985**, *107*, 5018. (j) Kumar, D.; Tahsini, L.; de Visser, S. P.; Kang, H. Y.; Kim, S. J.; Nam, W. *J. Phys. Chem. A* **2009**, *113*, 11713. (k) Das, A.; Grinkova, Y. V.; Sligar, S. G. *J. Am. Chem. Soc.* **2007**, *129*, 13778. (l) Byrn, M. P.; Katz, B. A.; Keder, N. L.; Levan, K. R.; Magurany, C. J.; Miller, K. M.; Pritt, J. W.; Strouse, C. E. *J. Am. Chem. Soc.* **1983**, *105*, 4916. (m) de Visser, S. P. *J. Biol. Inorg. Chem.* **2006**, *11*, 168. (n) de Visser, S. P. *J. Phys. Chem. B* **2007**, *111*, 12299. (o) Kumar, D.; de Visser, S. P.; Sharma, P. K.; Hirao, H.; Shaik, S. *Biochemistry* **2005**, *44*, 8148. (p) Meunier, B.; de Visser, S. P.; Shaik, S. *Chem. Rev.* **2004**, *104*, 3947. (q) Dey, A.; Okamura, T.; Ueyama, N.; Hedman, B.; Hodgson, K. O.; Solomon, E. I. *J. Am. Chem. Soc.* **2005**, *127*, 12046.
(9) (a) Chaudhary, A.; Patra, R.; Rath, S. P. *Eur. J. Inorg. Chem.* **2010**, 5211. (b) Sugimoto, H.; Ueda, N.; Mori, M. *Bull. Chem. Soc. Jpn.* **1982**, *55*, 3468. (c) Kanamori, D.; Yamada, Y.; Onoda, A.; Okamura, T.; Adachi, S.; Yamamoto, H.; Ueyama, N. *Inorg. Chim. Acta* **2005**, *358*, 331.
(10) Borovkov, V. V.; Hembury, G. A.; Inoue, Y. *Acc. Chem. Res.* **2004**, *37*, 449.
(11) Bussolo, V. D.; Caselli, M.; Romano, M. R.; Pineschi, M.; Crotti, P. *J. Org. Chem.* **2004**, *69*, 8702.
(12) (a) Guilard, R.; Tabard, A.; Caemelbecke, E. V.; Kadish, K. M. In *The Porphyrin Handbook*; Kadish, K. M., Smith, K. M., Guilard, R., Eds.; Academic Press: San Diego, CA, 2000; Vol. 3, Chapter 21, p 295. (b) Kadish, K. M.; Caemelbecke, E. V.; Gueletti, E.; Fukuzumi, S.; Miyamoto, K.; Suenobu, T.; Tabard, A.; Guilard, R. *Inorg. Chem.* **1998**, *37*, 1759.
(13) Weiss, R.; Gold, A.; Terner, J. *Chem. Rev.* **2006**, *106*, 2550.
(14) (a) Nakamura, M.; Ohgo, Y.; Ikezaki, A. *J. Inorg. Biochem.* **2008**, *102*, 433. (b) Nakamura, M. *Coord. Chem. Rev.* **2006**, *250*, 2271.
(15) (a) Walker, F. A. *Chem. Rev.* **2004**, *104*, 589. (b) Walker, F. A. *Coord. Chem. Rev.* **1999**, *186*, 471.
(16) (a) Schlichting, I.; Berendzen, J.; Chu, K.; Stock, A. M.; Maves, S. A.; Benson, D. E.; Sweet, R. M.; Ringe, D.; Petsko, G. A.; Sligar, S. G. *Science* **2000**, *287*, 1615. (b) Williams, P. A.; Cosme, J.; Ward, A.; Angove, H. C.; Vinković, D. M.; Jhoti, H. *Nature* **2003**, *424*, 464.
(17) Nakamura, K.; Ikezaki, A.; Ohgo, Y.; Ikeue, T.; Neya, S.; Nakamura, M. *Inorg. Chem.* **2008**, *47*, 10299.
(18) Ueyama, N.; Nishikawa, N.; Yamada, Y.; Okamura, T.; Oka, S.; Sakurai, H.; Nakamura, A. *Inorg. Chem.* **1998**, *37*, 2415.
(19) (a) Patra, R.; Sahoo, D.; Dey, S.; Sil, D.; Rath, S. P. *Inorg. Chem.* **2012**, *51*, 11294. (b) Patra, R.; Chaudhury, A.; Ghosh, S. K.; Rath, S. P. *Inorg. Chem.* **2010**, *49*, 2057. (c) Patra, R.; Bhowmik, S.; Ghosh, S. K.; Rath, S. P. *Dalton Trans.* **2010**, *39*, 5795. (d) Patra, R.; Chaudhury, A.; Ghosh, S. K.; Rath, S. P. *Inorg. Chem.* **2008**, *47*, 8324. (e) Patra, R.; Rath, S. P. *Inorg. Chem. Commun.* **2009**, *12*, 515. (f) Moore, K. T.; Fletcher, J. T.; Therien, M. J. *J. Am. Chem. Soc.* **1999**, *121*, 5196.
(20) Becke, A. D. *J. Chem. Phys.* **1993**, *98*, 5648.
(21) Lee, C.; Yang, W.; Parr, R. G. *Phys. Rev. B* **1988**, *37*, 785.
(22) Stevens, P. J.; Devlin, F. J.; Chabalowski, C. F.; Frisch, M. *J. Phys. Chem.* **1994**, *98*, 11623.
(23) Frisch, M. J.; Trucks, G. W.; Schlegel, H. B.; Scuseria, G. E.; Robb, M. A.; Cheeseman, J. R.; Montgomery, J. A., Jr.; Vreven, T.; Kudin, K. N.; Burant, J. C.; Millam, J. M.; Iyengar, S. S.; Tomasi, J.; Barone, V.; Mennucci, B.; Cossi, M.; Scalmani, G.; Rega, N.; Petersson, G. A.; Nakatsuji, H.; Hada, M.; Ehara, M.; Toyota, K.; Fukuda, R.; Hasegawa, J.; Ishida, M.; Nakajima, T.; Honda, Y.; Kitao, O.; Nakai, H.; Klene, M.; Li, X.; Knox, J. E.; Hratchian, H. P.; Cross, J. B.; Bakken, V.; Adamo, C.; Jaramillo, J.; Gomperts, R.; Stratmann, R. E.; Yazyev, O.; Austin, A. J.; Cammi, R.; Pomelli, C.; Ochterski, J. W.; Ayala, P. Y.; Morokuma, K.; Voth, G. A.; Salvador, P.; Dannenberg, J. J.; Zakrzewski, V. G.; Dapprich, S.; Daniels, A. D.; Strain, M. C.; Farkas, O.; Malick, D. K.; Rabuck, A. D.; Raghavachari, K.; Foresman, J. B.; Ortiz, J. V.; Cui, Q.; Baboul, A. G.; Clifford, S.; Cioslowski, J.; Stefanov, B. B.; Liu, G.; Liashenko, A.; Piskorz, P.; Komaromi, L.; Martin, R. L.; Fox, D. J.; Keith, T.; Al-Laham, M. A.; Peng, C. Y.; Nanayakkara, A.; Challacombe, M.; Gill, P. M. W.; Johnson, B.; Chen, W.; Wong, M. W.; Gonzalez, C.; Pople, J. A. *Gaussian 03*, revision B.04; Gaussian, Inc.: Pittsburgh, PA, 2003.
(24) Cheng, B.; Hobbs, J. D.; Debrunner, P. G.; Erlebacher, J.; Shelnutt, J. A.; Scheidt, W. R. *Inorg. Chem.* **1995**, *34*, 102.
(25) Hanwell, M. D.; Curtis, D. E.; Lonie, D. C.; Vandermeersch, T.; Zurek, E.; Hutchison, G. R. *J. Cheminf.* **2012**, *4*, 17.
(26) *SAINT+*, 6.02 ed.; Bruker AXS: Madison, WI, 1999.
(27) Sheldrick, G. M.; *SADABS 2.0*; Bruker AXS, Inc.: Madison, WI, 2000.
(28) Sheldrick, G. M. *Acta Crystallogr.* **2008**, *A64*, 112.